



Time-resolved Fourier transform infrared emission spectra of atomic Xenon: Newly measured Rydberg *g*-, *h*- and *i*-levels

S. Civiš^{a,*}, E.M. Zanozina^a, P. Kubelík^a, V.E. Chernov^b, A. Pastorek^a, M. Ferus^a

^a J. Heyrovský Institute of Physical Chemistry, Academy of Sciences of the Czech Republic, Dolejškova 3, 18223 Prague 8, Czech Republic

^b Voronezh State University, 394018 Voronezh, Russia

ARTICLE INFO

Keywords:

Time-resolved Fourier-transform spectroscopy

Infrared spectra

Rydberg levels

Xenon

Atomic data

ABSTRACT

The time-resolved Fourier transform technique was employed to record the spectrum of neutral xenon (Xe I) within a distinct spectral range of 700–14000 cm⁻¹ range. A complete series of up to one hundred scans were carried out and averaged to obtain a satisfactory signal-to-noise ratio with a resolution of 0.02 cm⁻¹, providing a detailed and high-quality representation of the xenon spectra. All existing observations of atomic Xe (1318 lines of which 111 are observed in this work for the first time) were included into the optimization procedure. As a result, we obtain an updated system of Xe I levels.

1. Introduction

Studying atomic Xe is important and relevant in various fields, including spectroscopy, radiative transfer, plasma diagnostics, laser physics, astrophysics, atomic physics, and potential technological applications. Xenon is also studied in the field of atomic physics, where it is used as a benchmark for theoretical calculations of atomic structure and interactions. The atomic Xe has potential applications in fields such as lighting, fluorescent displays, and plasma processing. Its unique properties, such as high ionization potential and low reactivity, make it a promising candidate for these applications.

Spectroscopic measurements on atomic Xe have been conducted for many years [1–5]. Broad understanding of atomic structure of Xe was first established in 1929 by Meggers [2] who photographed the Xe spectrum using a quartz-prism and a diffraction grating spectrometer in the wavenumber range from 9890 cm⁻¹ to 29,050 cm⁻¹ and reported 318 lines of neutral Xe. Further investigations in 1930 by Humphreys [3] extended the spectral range of observation to include both krypton and xenon. Humphreys employed a Fabry–Perot interferometer and glass discharge tubes as radiation sources to study the spectral range from 11,000 to 25,000 cm⁻¹. To improve the accuracy and precision of measurements, Humphreys and Meggers [6] re-examined the spectral range from 8000 to 30,000 cm⁻¹ using high-resolving power grating spectrometers and an interferometer. Their work had a wavelength accuracy of approximately 0.01–0.02 Å. In 1934, Meggers and Humphreys [4] further improved the precision (uncertainty within 0.001 Å) by performing interference measurements on the natural xenon spectrum in the photographic region. This study

covered 132 transitions with wavenumbers ranging from 10,075 to 25,320 cm⁻¹. Subsequently, in 1935, Meggers [5] added 25 additional Xe lines in the infrared range of 7500 to 9500 cm⁻¹. Humphreys and Kostkowski [7] investigated the range from 5900 to 8500 cm⁻¹ using a high-resolution grating spectrometer with 15,000 lines per inch and a lead-sulfide photo-conducting diode. Humphreys summarized the results of his various measurements in a compilation [8]. Mishra et al. [9] recorded Xe I spectra excited in a microwave discharge using Fourier transform spectroscopy (FTS) with an unapodized instrumental resolution of 0.1 cm⁻¹ and estimated the absolute accuracy of the measured wavenumbers to be better than 0.003 cm⁻¹ for strong transitions.

To combine and generalize the findings from these diverse measurements, Saloman created a critical compilation [10] which serves as the primary source for Xe I lines listed at National Institute of Standards and Technology Atomic Spectra Database (NIST ASD) [11].

However, the NIST ASD Xe I linelist does not spread beyond wavelengths longer than 5.5 μm, which is the InSb detector limit. Consequently, this linelist lacks infrared transitions involving Rydberg levels with high orbital momentum (*l* > 3), such as g-, h-, or i-levels. With liquid nitrogen cooled MCT (HgCdTe) detectors, the Fourier transform spectroscopy technique can be enhanced to observe transitions between these Rydberg levels in the mid-infrared domain, specifically below 1800 cm⁻¹.

The present study aims to investigate and report on these previously unobserved transitions, providing experimental energies of high-*l* Rydberg levels of neutral xenon. This research builds upon our previous

* Corresponding author.

E-mail address: civis@jh-inst.cas.cz (S. Civiš).

studies of high-resolution infrared (IR) spectra of noble gas atoms [12–15]. In this study, we have measured 335 lines of atomic Xe in the spectral range of 700–14,000 cm⁻¹ using Fourier transform infrared spectroscopy with a spectral resolution of 0.02 cm⁻¹.

2. Experimental details

To measure the Xe spectra in the range from 700 to 14,000 cm⁻¹, we have applied two discharge methods:

1. Alternating current (AC) discharge with time-resolved Fourier transform (FT) spectroscopy (700–7900 cm⁻¹). Due to software compatibility, our time resolved system is limited up to 7900 cm⁻¹.
2. Microwave (MW) discharge without the time resolution technique (700–14,000 cm⁻¹).

In our experiments the natural xenon (mixture of nine stable isotopes of Xe) was used. As it is shown in Refs. [16–18], the hyperfine splitting of Xe I levels and the isotope shift of Xe I transitions are of order of (or less than) 1 GHz ≈ 0.033 cm⁻¹, so these effects are not observable at our spectral resolution. Note that Ref. [16] reports on absolute frequency measurements of two lines (transitions from the ground state to 8d[1/2]_1 and 8d[3/2]_1) in ¹³⁶Xe and one line (transition from the ground state to 7s'[1/2]_1) in ¹³²Xe and measured isotope shifts of these lines in all isotopes present in natural xenon samples. From these measurements, one can derive the wavenumbers that should be observed in natural xenon, which was made by Saloman in his compilation [10]. For these three lines, which essentially define the connection of all excited level system to the ground level, we used Saloman's values. The VUV frequency-comb spectroscopy measurement [19] deals with ¹³²Xe isotope only. The isotope shift of this transition are needed for ¹²⁹Xe and ¹³¹Xe are needed to adapt the results of Ozawa and Kobayashi [19] to the natural Xe mixture, so we did not include this high-accuracy measurement result into our optimization.

2.1. Time-resolved fourier transform infrared spectroscopy

To investigate chemical reactions and dynamic properties of molecules, radicals, and ions, time-resolved spectroscopy is an efficient technique. In our study, we employed a special approach called synchronous scanning Fourier transform (FT) technique for time-resolved spectra analysis, particularly for phenomena lasting from microseconds to milliseconds [20]. This technique involves initiating the reaction in a pulsed mode, e. g. using a laser, electric discharge (utilized in this experiment), electron bombardment, or a hollow cathode [21]. More exploration of the FT technique applied to molecular measurement can be found in our previous research publications [22,23].

The data acquisition was performed using a modified Bruker IFS 120 spectrometer located at the J. Heyrovský Institute of Physical Chemistry [24]. Once a sufficient amount of data and scans were acquired, the time-shifted interferograms were composed. The modified Bruker IFS 120 spectrometer, adapted for time-resolved measurements, generated the scan's initiating signal, as well as the fringe signals of the He-Ne laser. These signals functioned as the system's time standard. The additional electronic signals crucial for synchronizing the measurement process, such as the discharge trigger and the analog-to-digital (AD) sampling trigger, were produced by the Field Programmable Gate Array (FPGA, Altera).

During the pulse excitation, our experimental setup continuously recorded the signal from the detector while the interferometer's mirror was continuously scanning. The entire measurement process was synchronized with He-Ne laser fringes. Fig. 1 illustrates the chart diagram of our time resolution and data acquisition system, providing a description of the time parameters used in our experiments. We set a measurement window limit of 100 μs, driven by the mirror speed of 10 kHz. The pulse width was specifically calibrated to 22 μs. The data

acquisition process comprised 30 data points with 3 μs offset after the beginning of the pulse. Each of the data points represents a complete recording across the entire spectral range at a distinct acquisition time. Data was acquired every 2nd microsecond, which covered a total acquisition window of 60 μs. Thanks to these configurations, we were able to record 10 spectra during the active pulse duration and 20 additional spectra in the post-discharge pulse phase. Our setup enabled us to take up to 30 time-resolved spectra with the spectral resolution ranging between 0.15 cm⁻¹ and 0.02 cm⁻¹ in one measurement. The time resolution achieved was approximately 1 μs, primarily limited by the bandwidth of the detector amplifier.

For more detailed information on the experimental setup, we refer to our previous papers [20,25,26].

2.2. Data acquisition

We employed two different methods to generate the xenon plasma in our experimental setup. The first method utilized a pulsed positive column discharge. A discharge tube with water-cooled stainless steel electrodes, measuring 20 cm in length and 12 mm in inner diameter, was filled with high-purity xenon gas (purity class 4.0: 99.990%). To achieve a strong emission spectrum, the xenon pressure was optimized at 0.5 torr. The discharge parameters applied across the electrodes were as follows: 1 kV voltage, 22 μs pulse width, and 100 mA peak-to-peak current.

The second method involved a microwave discharge operating at 2.45 GHz, which was used to generate the xenon plasma [27]. In this case, an electrodeless discharge lamp (EDL) was utilized as the emission source. The EDL was a 10 mm diameter and 8 cm long sealed tube filled with 0.5 torr of xenon. The microwave power varied from 15 to 25 watts. The EDL was cooled with dry ice to reduce the heat generated during the discharge and further cool the source.

The emitted radiation from both plasma generation methods was focused into a Bruker IFS 120 Fourier transform spectrometer, covering the spectral range of 700–14,000 cm⁻¹. The instrument was equipped with a KBr beam splitter and an HgCdTe (MCT) detector for the 700–2000 cm⁻¹ range, and a CaF₂ beam splitter and an InSb detector for the 2000–14,000 cm⁻¹ range. Different combinations of windows and lenses (a KBr window with a ZnSe lens and a CaF₂ window with a CaF₂ lens) were utilized depending on the spectral region of interest. Band pass interference filters (manufactured by Northumbria Optical Coatings Limited, UK) were used to improve the signal-to-noise ratio.

All the spectra were recorded with a non-apodized resolution of 0.02 cm⁻¹ and a time resolution of 1–2 μs. The resulting matrix contains 30 time-shifted interferograms (1 or 2 microsecond time shift) with the 22 microsecond discharge pulse duration at the beginning of the data acquisition process. Our system not only enables the time-resolved spectra measurement, but also provides 30 observed spectra that can be averaged to improve the signal-to-noise ratio. These averaged spectra were used for the analysis of each spectral line. The complete experimental parameters applied to the entire data acquisition process are presented in Table 1.

2.3. Wavenumber calibration

The wavenumber scale of the spectrum was calibrated using spectral lines of several molecular and atomic species (N₂O, CO, H₂O, NH₃, and Xe I). Most of the spectra used for the calibration were measured in absorption (the only exceptions were the CO and Xe observed in emission). A cell filled with the calibration gas (pressure ~2 torr) was placed in the sample chamber of the spectrometer and the spectrum with the Xe discharge as the radiation source was measured. A few H₂O lines at the atmospheric pressure (outside the spectrometer) were also used. In the spectral range above 2000 cm⁻¹ an IR-lamp was utilized as an additional radiation source because of the low intensity of the discharge's black body radiation in this region. For the calibration

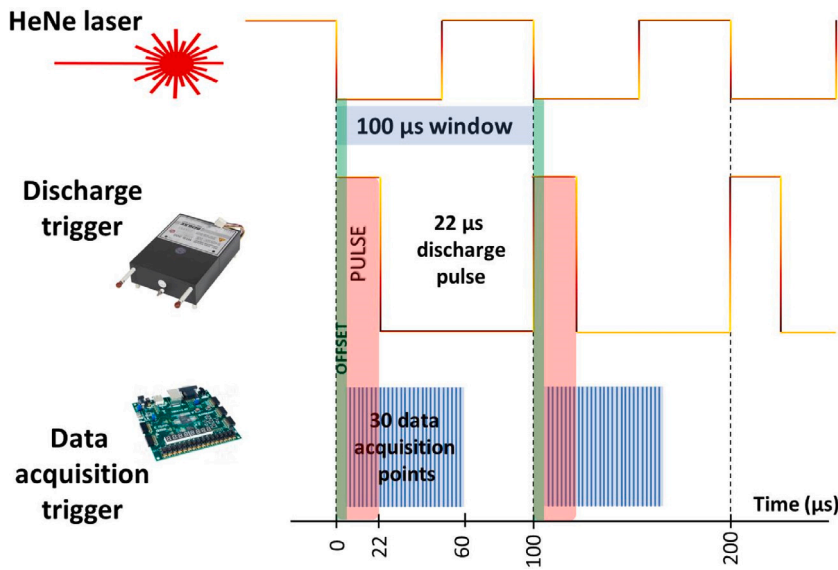


Fig. 1. Chart diagram of the time resolution and data acquisition system. Each measurement window was limited to 100 μ s because of 10 kHz mirror speed. Pulse width was set to 22 μ s. The data acquisition consisted of 30 acquisition points with 3 μ s offset, each point being a full spectrum in the whole spectral range at a specified time of acquisition. Acquisition was set to each 2nd microsecond, thus covering a 60- μ s acquisition window. Because of these particular settings, 10 spectra were recorded within the pulse duration and 20 spectra after the discharge pulse period.

Table 1
Single-measurement spectral ranges and instrument configuration.

Spectral range (cm^{-1})	Method of discharge	Windows	Northumbria Optical Coatings Limited Filter specification	Detector	Beam splitter	Lens
700–1000	AC	KBr	WBP 3067	MCT	KBr	ZnSe
1000–1250	AC	KBr	WBP 3067	MCT	KBr	ZnSe
1250–1600	AC	KBr	WBP 3067	MCT	KBr	ZnSe
1600–2000	AC	CaF_2	WBP 3067	InSb	CaF_2	CaF_2
2000–4000	AC	CaF_2	LWP 3673	InSb	CaF_2	CaF_2
4000–5000	AC	CaF_2	WBP 3834	InSb	CaF_2	CaF_2
5000–7700	AC	CaF_2	WBP 4187	InSb	CaF_2	CaF_2
7700–14,000	EDL	CaF_2	no filter	InSb	CaF_2	CaF_2

we used a set of spectra measured during the whole experimental campaign. More than 200 spectral lines were used for the calibration to cover the entire spectral range of this experiment. The spectral lines used for the calibration belong to the following vibration bands: N_2O (02°0–00°0, 10°1–00°0), CO (2–1, 4–2, 1–0, 3–1,), H_2O (010–000, 001–000), NH_3 (0100–0000, 0200–0100), and Xe I (lines listed in the NIST ASD [11]) for the spectral range up to 5000 cm^{-1} and N_2O (20°1–00°0, 00°2–00°0), CO (4–2, 3–1), and Xe I (lines listed in the NIST ASD [11]) for the range 5000–12,000 cm^{-1} . The data used for the calibration were included in the supplementary online material. The high-precision reference wavenumbers of the above molecular lines were taken from the HITRAN database [28]. The typical uncertainties of the reference HITRAN wavenumbers are: $\Delta\nu_{\text{ref}}(\text{N}_2\text{O}) \sim 0.001 \text{ cm}^{-1}$, $\Delta\nu_{\text{ref}}(\text{CO}) \sim 0.001 \text{ cm}^{-1}$ $\Delta\nu_{\text{ref}}(\text{NH}_3) \sim 0.0001 \text{ cm}^{-1}$.

The calibration was performed by linearly fitting ($W_{\text{corrected}} = W_{\text{observed}} - (\alpha * W_{\text{observed}} + \beta)$) the observed line positions to the reference high-precision wavenumber values from the HITRAN [28], HITEMP [29], and NIST ASD [11] databases (see Fig. 2). The obtained calibration factors were small, having little effect on the most of the resulting wavenumbers listed in Table 2. The wavenumber correction factors with their uncertainties are as follows:

- spectral range 800–5000 cm^{-1} : $\alpha = 3.00 \cdot 10^{-7}$, $\Delta\alpha = 1.27 \cdot 10^{-7}$; $\beta = -5.06 \cdot 10^{-3}$, $\Delta\beta = 2.01 \cdot 10^{-4}$
- spectral range 5000–12,000 cm^{-1} : $\alpha = 1.56 \cdot 10^{-7}$, $\Delta\alpha = 1.33 \cdot 10^{-7}$; $\beta = 3.28 \cdot 10^{-3}$, $\Delta\beta = 1.10 \cdot 10^{-3}$.

The error bars in Fig. 2 show the observed uncertainties,

$$\Delta\nu_{\text{obs}} = \sqrt{(\Delta\nu_{\text{stat}})^2 + (\Delta\nu_{\text{ref}})^2}, \quad (1)$$

where $\Delta\nu_{\text{ref}}$ are the uncertainties of the reference line wavenumbers. The statistical uncertainties, $\Delta\nu_{\text{stat}}$, are supposed to be the maximal value: $\Delta\nu_{\text{stat}} = \max\{\Delta\nu_{\text{Brault}}, \Delta\nu_{\text{fit}}\}$, where $\Delta\nu_{\text{Brault}}$ is determined by the general expression (2) for the line position error according to [30]:

$$\Delta\nu_{\text{Brault}} = \frac{W}{\text{SNR} N_W^{1/2}} \quad (2)$$

where SNR is signal-to-noise ratio, W is the full width at half maximum (FWHM) and N_W is the number of statistically-independent data points per W . The uncertainties $\Delta\nu_{\text{fit}}$ are errors due to fitting the measured data arrays to a Lorentzian or Gaussian line profile. The fit and the estimation of the corresponding statistical uncertainties $\Delta\nu_{\text{fit}}$ can be obtained using any software for data visualization (e. g., Origin) or scientific calculation (e. g., Mathematica).

Full uncertainties of the measured wavenumber were calculated by adding the observed (1) and calibration uncertainties in quadrature, $\Delta\nu = \sqrt{(\Delta\nu_{\text{obs}})^2 + (\Delta\nu_{\text{Brault}})^2 + (\Delta\nu_{\text{fit}})^2}$, where α and β are the parameters obtained by fitting the wavenumber deviations of the reference lines (see Fig. 2).

For the wavelengths calibration several spectra recorded before as well as after the measurement of the spectra used for the analysis in this work. So that all the data are calibrated by two sets of the calibration parameters belonging to two spectral regions, 800–5000 and 5000–12,000 cm^{-1} .

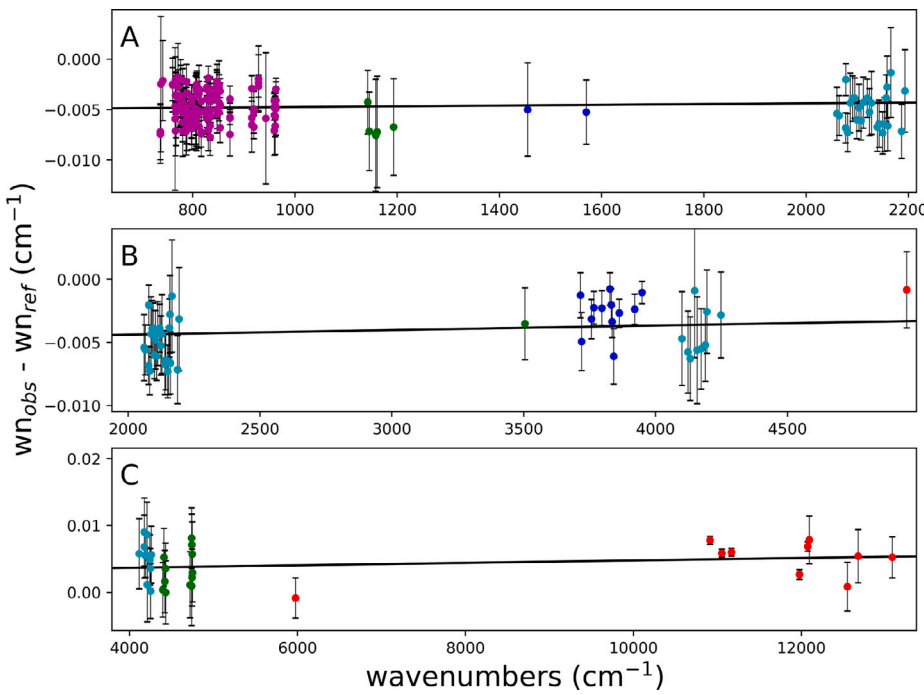


Fig. 2. Differences between the observed and reference spectral line positions used for the wavenumber calibration. The various colors correspond to different species: green — N₂O, blue — H₂O, cyan — CO, magenta — NH₃, and red — Xe I. The black line shows the fitted linear calibration function. Panel A and B show a single calibration plot split into two parts for better readability. Panel C is a separate calibration plot.

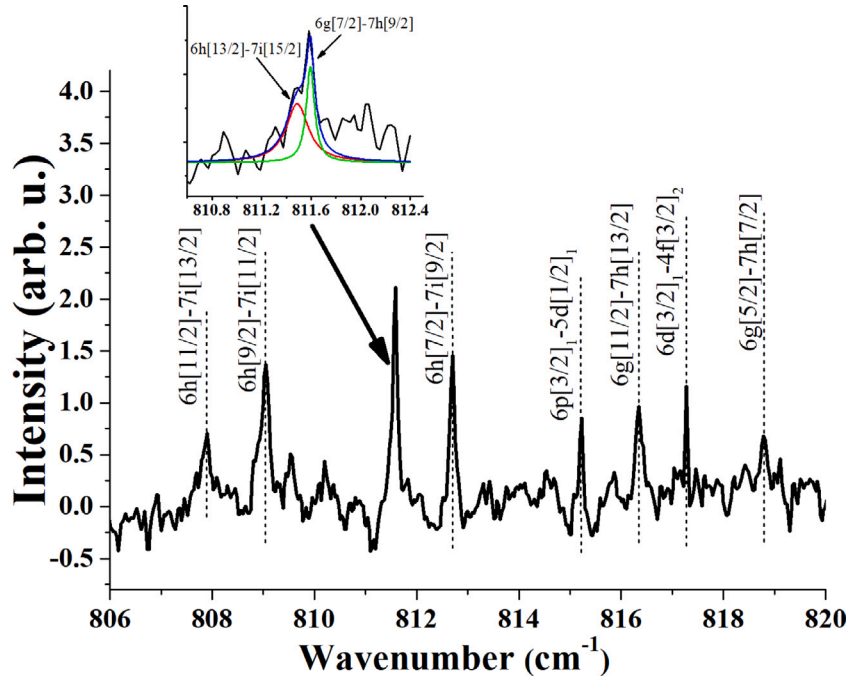


Fig. 3. 6h-7i and 6g-7h transitions lines near 815 cm⁻¹ in measured spectrum.

3. Results and discussion

As a result, 335 spectral lines of Xe I were detected in the entire spectral range of 700–14,000 cm⁻¹. Among these lines, 111 are identified for the first time, and most of these appeared in the spectral region below the 2500 cm⁻¹.

The observed and fitted spectral lines of the 6h-7i and 6g-7h transitions near the 815 cm⁻¹ spectral region are displayed in Fig. 3.

As an example, the time-resolved spectrum of the 5g-6h transitions of Xe I near 1340 cm⁻¹ is depicted in Fig. 4.

To obtain the line parameters, such as wavenumbers of the line positions, intensities and line widths, the lines measured in the AC discharge were fitted with Lorentzian profiles, and lines obtained in the microwave discharge were fitted with a Gaussian profile. For identification, we use the $J_1 l$ -coupling notation. For example, the notation $6p[3/2]_1$ in Table 2 means $5p^5(^2P_{1/2})6p^2[3/2]_1$ and the final term in such coupling scheme results from coupling the parent-level $J_1 = 1/2$ to

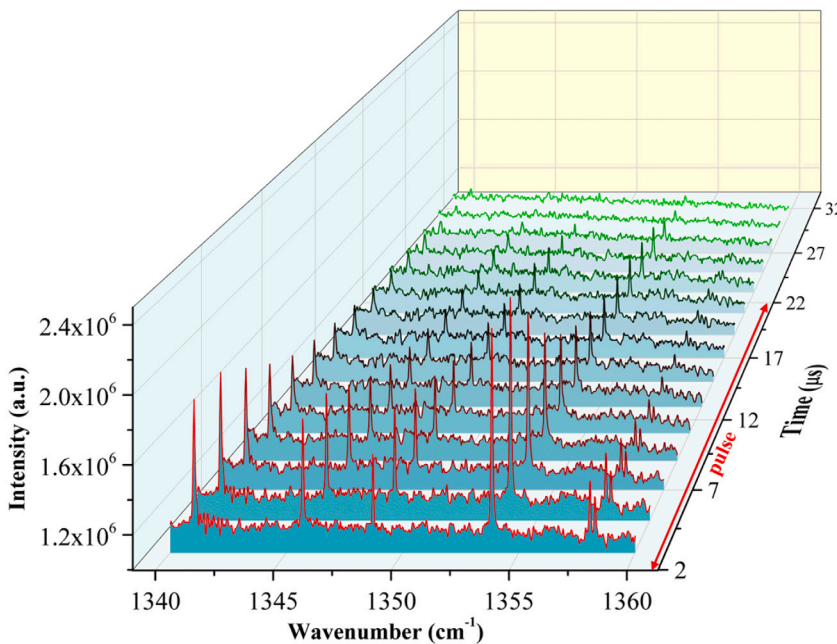
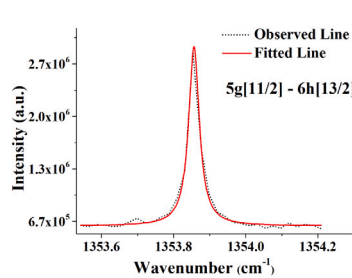
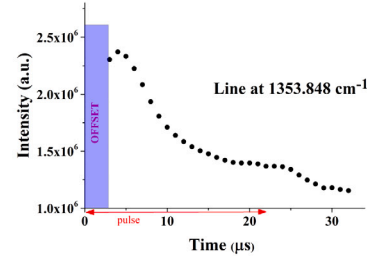
(a) The time profile of 5g–6h transitions in 1340–1360 cm⁻¹ spectral range.(b) Lorentzian fitted profile for the observed line at 1353.8 cm⁻¹.(c) Temporal decay of the 1353.8 cm⁻¹ line during the 22 microsecond time duration of the discharge pulse (1 μs sampling method).

Fig. 4. The time-resolved spectra of Xe I near 1350 cm⁻¹ spectral range. Spectra were recorded with 22 μs pulse width and 30 μs data acquisition window. A small bump on the time profile curve (25 μs) in Fig. 4(c) is probably caused by multi-level deexcitation via various relaxation paths, thus resulting in secondary excitations.

the orbital angular momentum of the 6p electron to obtain the resultant $K = 3/2$ (the K value is enclosed in brackets). The spin of the external electron ($2S + 1 = 2$) is then coupled with the K angular momentum to obtain a pair of J values, $J = K \pm 1/2$ (see the Notations for Different Coupling Schemes Section of Ref. [31]). Table 2 lists all our observed and classified lines involving transitions between $5p^5(^2P_{1,3})nl^2[K]_J$ levels with $n = 4\text{--}9$. The measurements were performed in different spectral ranges: 700–1000, 1000–1200, 1200–1800, 1800–2000, 2000–4000, 4000–5000, 5000–7700, 7700–14,000 cm⁻¹. The arbitrary units of intensity I_{ki} are valid only within the same spectral range because we used different combinations of detectors and optics to cover the entire range (see Table 1).

The uncertainties (on the level of one standard deviation) of the measured lines presented in Table 2 are given in parentheses (for example, 123.4(56) means 123.4 ± 5.6).

The last column in Table 2 presents the wavenumbers of Xe I obtained from previous measurements. The uncertainties in wavenumbers for the measured values are taken from Table 3 of Saloman [10]. In general, our results are in agreement with those from prior studies, taking into account the reported uncertainties.

To extract the energies of Xe I levels from the measured line wavenumbers we used the LOPT program [38]. This software executes a least-square optimization of the level energies to minimize the

total of squared differences between the observed and Ritz values. The precision of the fit is strongly correlated with the quality and fullness of the spectral lines input set for the fitting process. Thus, it is important to gather as much spectral data from literature as possible for xenon atom, limited by laboratory observations only (theoretical calculations were not included). In our study, we compiled spectral data from various literature sources [4–9,16,32–35,37,39–45] for the Xe atom. These data comprise 1318 lines; the complete list of lines with classifications, uncertainties, observed–Ritz differences and references is available as a supplementary online material.

The internal consistency of our measured wavenumbers presented in Table 2 was inspected by calculating the reduced residuals, $R_i = (\sigma_{\text{obs},i} - \sigma_{\text{calc},i})/u_i$. For a specific line i , this metric is computed as the difference between the observed wavenumber ($\sigma_{\text{obs},i}$) and the computed Ritz wavenumber ($\sigma_{\text{calc},i}$), normalized by the uncertainty of the observed wavenumber (u_i). The reduced residuals R_i are plotted as a function of the corresponding normal order statistic medians which are defined as $G(U_i)$ [46]. Here U_i represents the expected value of the i th order statistic in an array of size n from a uniform distribution on the interval [0,1]. The function G is the inverse of the standard normal cumulative distribution function (CDF). So, the normal probability plot is constructed by plotting the reduced residuals R_i against the corresponding $G(U_i)$ values. $G(U_i)$ in our case depends only on number

Table 2

Xe IR line wavenumbers ν_{ki} , intensities I_{ki} , signal-to-noise ratios (SNR) and full widths at half-maxima (FWHM). The measurements were performed in different spectral ranges: 700–1000, 1000–1200, 1200–1800, 1800–2000, 2000–4000, 4000–5000, 5000–7700, 7700–14 000 cm⁻¹. The arbitrary units of intensity are valid only within the same spectral range. Description of literature abbreviations in column 'Other work': [L1975] [32]; [L234] [33]; [L2228] [8]; [L4227c110] [34]; [L9760] [9]; [L7384] [7]; [L7293] [5]; [L7292] [4]; [L4739] [6]; [L4085] [35]; [L4211c2] [36]; [L7449] [37].

ν_{ki} (cm ⁻¹)	I_{ki} (arb. u.)	SNR	FWHM (cm ⁻¹)	Identification	Other work (if any)
732.070(15)	2.46×10^6	10.2	0.077(13)	$7d[7/2]_3-5f[9/2]_4$	
742.283(10)	1.22×10^5	3.18	0.076(20)	$7d[5/2]_3-5f[7/2]_3$	
774.148(22)	2.86×10^6	5.42	0.060(21)	$6p[3/2]_2-5d[1/2]_1$	
781.336(11)	1.15×10^5	3.40	0.056(21)	$7p[1/2]_1-6d[3/2]_2$	
792.008(13)	1.44×10^5	3.20	0.141(27)	$9s[3/2]_2-9p[3/2]_2$	
807.894(17)	9.37×10^5	2.90	0.149(38)	$6h[11/2]_3-7i[13/2]$	
809.041(9)	4.07×10^6	2.60	0.213(22)	$6h[9/2]_2-7i[11/2]$	
811.598(23)	1.82×10^6	7.45	0.082(63)	$6h[13/2]_2-7i[15/2]$	
812.705(30)	1.34×10^6	5.50	0.119(28)	$6h[7/2]_2-7i[9/2]$	
815.223(19)	1.19×10^6	6.13	0.063(18)	$6p[3/2]_1-5d[1/2]_0$	
816.350(12)	1.58×10^6	5.43	0.163(18)	$6g[11/2]_2-7h[13/2]$	
817.281(14)	9.54×10^5	7.44	0.053(12)	$6d[3/2]_1-4f[3/2]_2$	
818.799(27)	8.35×10^4	2.41	0.128(89)	$6g[5/2]_2-7h[7/2]$	
848.069(5)	1.02×10^7	21.2	0.061(5)	$7p[3/2]_2-6d[5/2]_3$	
864.137(7)	2.12×10^6	14.9	0.077(7)	$6p'[3/2]_1-6d[5/2]_2$	
877.893(5)	3.65×10^6	18.1	0.056(5)	$6d[3/2]_1-4f[5/2]_2$	
891.579(5)	3.98×10^6	23.1	0.061(5)	$7p[5/2]_2-6d[5/2]_2$	
912.031(30)	9.23×10^5	3.69	0.054(28)	$5f[9/2]_4-8d[7/2]_3$	
918.614(8)	8.18×10^4	4.16	0.063(17)	$5f[7/2]_3-8d[5/2]_2$	
923.442(17)	1.43×10^6	6.31	0.082(15)	$5d'[3/2]_2-8p[3/2]_2$	
932.542(5)	1.34×10^7	37.9	0.068(2)	$7a[7/2]_4-5f[9/2]_5$	
949.086(21)	9.46×10^5	6.78	0.096(20)	$5f[7/2]_4-8d[5/2]_3$	
1065.359(7)	1.14×10^4	5.96	0.051(16)	$7p[5/2]_3-6d[5/2]_3$	
1072.371(3)	5.20×10^4	9.51	0.056(11)	$6s'[1/2]_0-6p[1/2]_1$	
1110.281(5)	4.76×10^5	6.97	0.078(8)	$6p[3/2]_2-5d[3/2]_2$	
1133.300(3)	1.62×10^4	8.53	0.048(13)	$8p[5/2]_3-9s[3/2]_2$	
1189.901(5)	1.52×10^4	10.1	0.049(10)	$7p[1/2]_0-6d[3/2]_1$	
1287.599(4)	5.49×10^5	15.2	0.065(15)	$7p[3/2]_1-6d[3/2]_1$	
1288.928(9)	1.22×10^6	23.9	0.027(2)	$8s[3/2]_1-8p[5/2]_2$	
1326.942(5)	6.44×10^5	16.1	0.035(4)	$6d[5/2]_3-4f[9/2]_4$	
1341.044(5)	1.10×10^6	29.1	0.058(5)	$5g[9/2]_2-6h[11/2]$	
1345.730(5)	1.06×10^6	29.0	0.052(5)	$5g[7/2]_2-6h[9/2]$	
1348.740(5)	8.19×10^5	17.9	0.046(5)	$8s[3/2]_2-8p[1/2]_1$	
1353.861(4)	1.94×10^6	31.5	0.043(3)	$5g[11/2]_2-6h[13/2]$	
1358.082(6)	4.93×10^5	9.85	0.035(5)	$5g[5/2]_3-6h[7/2]_4$	
1358.297(7)	3.90×10^5	7.48	0.039(6)	$5g[5/2]_2-6h[7/2]_3$	
1364.950(6)	3.36×10^4	8.05	0.083(18)	$5f[7/2]_4-6g[9/2]_5$	
1365.030(8)	7.90×10^3	5.22	0.030(17)	$5f[7/2]_3-6g[9/2]_4$	
1366.717(3)	3.51×10^6	17.6	0.035(3)	$6p[3/2]_1-5d[3/2]_2$	
1372.509(12)	2.74×10^5	8.05	0.044(11)	$6d[5/2]_3-4f[5/2]_3$	
1378.249(4)	2.81×10^4	7.17	0.039(16)	$5f[5/2]_2-6g[7/2]_3$	
1380.746(5)	1.67×10^4	7.39	0.045(11)	$5f[5/2]_3-6g[7/2]_4$	
1396.831(11)	2.68×10^5	8.65	0.058(10)	$5f[9/2]_4-6g[11/2]_5$	
1397.559(8)	3.58×10^5	8.74	0.041(7)	$5f[9/2]_5-6g[11/2]_6$	
1400.639(6)	5.56×10^5	15.2	0.035(6)	$8s[3/2]_1-8p[3/2]_1$	
1405.350(15)	1.51×10^5	6.23	0.028(13)	$5f[3/2]_2-6g[5/2]_3$	
1409.570(2)	4.02×10^6	44.5	0.029(2)	$6d[5/2]_3-4f[7/2]_4$	
1438.483(8)	3.16×10^5	10.4	0.033(7)	$8s[3/2]_1-8p[3/2]_2$	
1460.411(4)	1.74×10^6	18.8	0.045(3)	$8s[3/2]_2-8p[5/2]_3$	
1566.381(2)	2.91×10^4	24.6	0.025(2)	$8s[3/2]_2-8p[3/2]_2$	
1584.281(2)	3.28×10^5	40.0	0.022(2)	$4f[9/2]_5-7d[7/2]_4$	
1666.806(2)	7.30×10^4	26.0	0.023(11)	$6d[5/2]_2-4f[5/2]_2$	
1700.793(2)	2.44×10^5	9.06	0.024(6)	$6d[5/2]_2-4f[7/2]_3$	
1784.623(3)	2.00×10^5	5.51	0.027(10)	$4f[9/2]_4-7d[7/2]_3$	
1789.468(4)	2.46×10^5	3.97	0.036(12)	$4f[7/2]_4-7d[5/2]_3$	
1793.568(2)	6.71×10^7	10.2	0.032(2)	$6p[5/2]_3-5d[7/2]_4$	
1836.616(2)	4.61×10^6	15.5	0.029(2)	$6d[7/2]_3-4f[9/2]_4$	1836.64(13) [L1975]
1866.820(2)	2.42×10^5	7.47	0.022(7)	$6p[5/2]_2-5d[1/2]_1$	
1919.157(2)	6.02×10^5	6.70	0.026(8)	$6d[7/2]_3-4f[7/2]_3$	1919.20(15) [L1975]
1919.238(11)	8.51×10^5	4.65	0.049(18)	$6d[7/2]_3-4f[7/2]_4$	1919.20(15) [L1975]
1948.958(10)	2.95×10^5	6.20	0.036(9)	$6d[7/2]_4-4f[9/2]_5$	1949.00(11) [L1975]
1961.369(19)	2.96×10^4	5.22	0.026(18)	$8p[5/2]_3-8d[7/2]_4$	1961.39(15) [L1975]
1999.070(13)	6.31×10^4	5.86	0.037(12)	$8p[3/2]_2-8d[5/2]_3$	1999.13(16) [L1975]
2027.421(17)	7.42×10^4	5.22	0.037(17)	$6s'[1/2]_1-6p[3/2]_2$	2027.46(12) [L1975]
2032.441(9)	5.40×10^5	5.48	0.050(8)	$6d[7/2]_4-4f[7/2]_4$	2032.46(17) [L1975]
2068.865(11)	3.69×10^5	7.89	0.047(11)	$8p[5/2]_2-8d[7/2]_3$	2068.85(17) [L1975]
2074.723(12)	9.55×10^4	4.95	0.051(11)	$8p[1/2]_1-8d[1/2]_1$	2075.06(17) [L1975]
2090.170(11)	1.92×10^5	4.70	0.061(9)	$7p[1/2]_0-8s[3/2]_1$	2090.20(17) [L1975]

(continued on next page)

Table 2 (continued).

ν_{ki} (cm ⁻¹)	I_{ki} (arb. u.)	SNR	FWHM (cm ⁻¹)	Identification	Other work (if any)
2118.039(10)	4.50×10^5	4.90	0.052(9)	$8p[5/2]_2-8d[5/2]_2$	2118.07(18) [L1975]
2140.972(7)	6.54×10^5	6.48	0.062(6)	$6d[3/2]_2-4f[3/2]_2$	2141.03(18) [L1975]
2154.324(6)	1.32×10^5	8.15	0.035(6)	$5g[7/2]_2-7h[9/2]$	
2164.025(6)	9.87×10^4	8.59	0.023(5)	$5g[11/2]_2-7h[13/2]$	
2168.767(9)	3.84×10^5	8.73	0.047(8)	$6p'[1/2]_1-5d'[3/2]_2$	2168.79(19) [L1975]
2187.874(11)	7.56×10^5	4.73	0.054(9)	$7p[3/2]_1-8s[3/2]_1$	2187.90(19) [L1975]
2198.622(12)	3.94×10^6	4.61	0.054(10)	$6d[3/2]_2-4f[5/2]_3$	2168.68(15) [L1975]
2201.584(10)	1.74×10^5	6.62	0.037(9)	$6d[3/2]_2-4f[5/2]_2$	2201.58(19) [L1975]
2202.949(13)	1.91×10^5	6.97	0.053(13)	$6p[5/2]_2-5d[3/2]_2$	2202.97(10) [L1975]
2245.935(9)	2.74×10^5	7.23	0.056(8)	$7p[3/2]_2-8s[3/2]_1$	2246.0(2) [L1975]
2268.142(17)	1.14×10^5	4.31	0.041(4)	$5d'[5/2]_2-5f[7/2]_3$	2268.3(2) [L1975]
2268.273(17)	1.17×10^5	4.69	0.053(3)	$6p'[1/2]_0-7d[1/2]_1$	2268.3(2) [L1975]
2290.004(9)	3.97×10^5	4.65	0.065(6)	$6d[1/2]_1-4f[3/2]_1$	2290.01(21) [L1975]
2299.665(7)	7.45×10^5	5.68	0.070(5)	$6d[1/2]_1-4f[3/2]_2$	2299.66(16) [L1975]
2300.904(14)	2.48×10^4	5.09	0.044(13)	$6d[3/2]_1-8p[3/2]_1$	2300.9(2) [L1975]
2335.328(9)	1.49×10^6	6.78	0.055(8)	$7p[5/2]_3-8s[3/2]_1$	2335.31(16) [L1975]
2348.758(8)	5.14×10^5	6.55	0.068(6)	$6d[1/2]_0-4f[3/2]_1$	2348.80(17) [L1975]
2360.277(9)	1.10×10^5	5.61	0.049(7)	$6d[1/2]_1-4f[5/2]_2$	2360.3(2) [L1975]
2408.114(20)	3.47×10^5	4.31	0.078(19)	$7p[3/2]_1-5d'[5/2]_2$	2408.13(16) [L1975]
2425.421(18)	3.72×10^4	4.14	0.059(16)	$6p[3/2]_1-8s[3/2]_2$	2425.41(24) [L1975]
2452.862(10)	3.15×10^5	4.94	0.053(8)	$7p[5/2]_2-8s[3/2]_2$	2452.84(6) [L234]
2466.164(15)	1.24×10^4	5.42	0.031(15)	$7p[3/2]_2-5d'[5/2]_2$	2466.13(24) [L1975]
2487.117(10)	3.11×10^5	5.01	0.056(9)	$7s[3/2]_1-7p[1/2]_1$	2487.12(6) [L234]
2495.612(8)	2.86×10^5	5.70	0.089(4)	$4f[7/2]_4-5g[7/2]_4$	2495.59(6) [L234]
2495.704(22)	2.05×10^5	4.41	0.082(20)	$4f[7/2]_3-5g[7/2]_3$	2495.59(6) [L234]
2501.915(13)	8.60×10^4	3.05	0.053(10)	$4f[7/2]_4-5g[9/2]_5$	2502.06(6) [L234]
2501.997(87)	3.93×10^4	2.90	0.036(84)	$4f[7/2]_3-5g[9/2]_4$	2502.06(6) [L234]
2502.130(7)	2.36×10^5	9.15	0.056(7)	$6p[1/2]_1-5d[1/2]_0$	2502.15(6) [L234]
2511.232(11)	4.84×10^5	6.81	0.076(10)	$4f[5/2]_2-5g[5/2]_2$	2511.18(6) [L234]
2514.405(8)	8.21×10^5	5.14	0.083(4)	$4f[5/2]_3-5g[5/2]_3$	2514.45(6) [L234]
2522.977(10)	3.15×10^5	5.25	0.053(8)	$6d[3/2]_1-8p[1/2]_0$	2523.0(3) [L1975]
2529.697(10)	5.69×10^6	4.87	0.056(8)	$4f[5/2]_2-5g[7/2]_3$	2529.73(6) [L234]
2532.656(10)	7.99×10^6	4.87	0.057(8)	$4f[5/2]_3-5g[7/2]_4$	2532.68(6) [L234]
2553.309(12)	3.49×10^5	4.97	0.055(11)	$6p'[3/2]_1-8s[3/2]_1$	2553.292(65) [L234]
2565.854(9)	1.01×10^7	8.42	0.052(8)	$4f[9/2]_4-5g[11/2]_3$	2565.87(7) [L234]
2566.708(13)	1.39×10^7	10.8	0.059(13)	$4f[9/2]_5-5g[11/2]_6$	2566.76(7) [L234]
2567.381(15)	6.87×10^6	5.75	0.051(14)	$6p[5/2]_3-5d[7/2]_3$	2567.368(66) [L234]
2572.054(10)	1.30×10^6	4.54	0.057(8)	$4f[3/2]_2-5g[5/2]_3$	2572.10(7) [L234]
2580.753(9)	7.35×10^5	6.86	0.057(7)	$7p[5/2]_2-8s[3/2]_1$	2580.738(67) [L234]
2581.508(9)	8.33×10^5	4.88	0.059(7)	$4f[3/2]_1-5g[5/2]_2$	2581.46(7) [L234]
2584.211(10)	5.91×10^5	4.73	0.061(7)	$6p'[3/2]_2-5d'[5/2]_3$	2584.190(67) [L234]
2584.557(13)	1.16×10^5	3.35	0.057(10)	$4f[9/2]_4-5g[11/2]_4$	2584.60(7) [L234]
2585.403(7)	1.82×10^5	6.50	0.069(5)	$4f[9/2]_5-5g[9/2]_5$	2585.39(7) [L234]
2596.945(24)	3.73×10^4	4.21	0.10(22)	$8s[3/2]_2-5f[5/2]_3$	2596.8(3) [L1975]
2683.444(80)	4.48×10^4	5.04	0.066(18)	$7p[5/2]_1-5d'[5/2]_2$	2683.5(3) [L1975]
2713.049(10)	4.87×10^5	4.74	0.056(8)	$6p[3/2]_2-5d[5/2]_2$	2713.1(2) [L1975]
2717.473(7)	3.49×10^6	6.58	0.064(6)	$6p[1/2]_1-5d[1/2]_1$	2717.48(7) [L1975]
2730.382(11)	2.42×10^4	7.15	0.045(11)	$6d[5/2]_3-8p[5/2]_3$	2730.4(3) [L1975]
2738.355(7)	2.91×10^6	5.46	0.081(3)	$7s[3/2]_1-7p[1/2]_1$	2738.34(8) [L1975]
2759.252(6)	1.08×10^5	17.2	0.061(5)	$6s'[1/2]_0-6p[3/2]_1$	2759.26 [L2228]
2760.978(12)	3.73×10^5	12.3	0.060(11)	$7p[3/2]_2-5d'[3/2]_2$	2760.97 [L2228]
2836.350(9)	2.72×10^5	6.12	0.067(8)	$6d[5/2]_3-8p[3/2]_2$	2836.36 [L2228]
2850.640(9)	3.68×10^7	6.97	0.056(8)	$6p[5/2]_2-5d[7/2]_3$	
2877.410(7)	7.87×10^5	6.24	0.066(6)	$7p[1/2]_1-8s[3/2]_2$	2877.41 [L2228]
2911.664(9)	3.38×10^6	4.72	0.061(7)	$7s[3/2]_1-7p[5/2]_2$	2912.06(85) [L4227c110]
2933.915(16)	1.19×10^5	6.81	0.046(15)	$6s'[1/2]_1-6p[1/2]_0$	2933.92 [L2228]
2939.111(12)	4.26×10^5	4.83	0.059(11)	$7s[3/2]_1-6p'[3/2]_1$	2939.11 [L2228]
2969.481(8)	1.77×10^7	7.25	0.056(7)	$6p[3/2]_1-5d[5/2]_2$	
2978.100(18)	3.39×10^4	5.02	0.029(17)	$6d[5/2]_3-8p[5/2]_2$	2978.26 [L2228]
3005.307(12)	2.37×10^5	5.83	0.058(11)	$7p[1/2]_1-8s[3/2]_1$	3005.30 [L2228]
3053.606(8)	3.60×10^6	6.40	0.066(6)	$6p[1/2]_1-5d[3/2]_2$	
3089.804(11)	2.89×10^5	4.69	0.058(9)	$6d[5/2]_2-8p[3/2]_1$	3089.81 [L2228]
3095.796(19)	2.66×10^5	4.52	0.051(18)	$7p[5/2]_2-5d'[3/2]_2$	3095.79 [L2228]
3162.903(10)	4.80×10^6	4.99	0.055(9)	$7s[3/2]_2-7p[5/2]_2$	3162.91 [L2228]
3190.345(10)	5.27×10^5	6.21	0.066(8)	$7s[3/2]_2-6p'[3/2]_1$	3190.35 [L2228]
3196.471(9)	5.33×10^5	7.04	0.057(8)	$6d[7/2]_3-8p[5/2]_2$	3196.47 [L2228]
3217.739(9)	4.17×10^7	6.64	0.056(8)	$6p[3/2]_2-5d[5/2]_3$	
3240.056(24)	8.42×10^4	3.99	0.070(22)	$6d[7/2]_3-8p[5/2]_3$	3240.06 [L2228]
3246.482(10)	4.52×10^6	4.95	0.057(8)	$7s[3/2]_1-7p[3/2]_2$	3246.48 [L2228]
3277.353(18)	2.62×10^5	5.22	0.049(17)	$7p[5/2]_1-5d'[5/2]_3$	3277.36 [L2228]
3280.436(7)	2.49×10^7	7.43	0.058(6)	$7s[3/2]_2-7p[5/2]_3$	
3286.034(17)	1.91×10^5	4.05	0.053(15)	$7p[1/2]_0-7d[1/2]_1$	3286.03 [L2228]
3304.543(8)	4.10×10^6	6.88	0.061(7)	$7s[3/2]_1-7p[3/2]_1$	3304.54 [L2228]
3330.006(17)	1.22×10^5	5.58	0.057(16)	$8s[3/2]_2-9p[5/2]_3$	3329.99 [L2228]

(continued on next page)

Table 2 (continued).

ν_{ki} (cm ⁻¹)	I_{ki} (arb. u.)	SNR	FWHM (cm ⁻¹)	Identification	Other work (if any)
3334.082(11)	2.62×10^5	5.48	0.069(9)	$6d[3/2]_1-5f[3/2]_2$	3334.09 [L2228]
3353.255(8)	7.40×10^5	7.26	0.056(7)	$6d[7/2]_4-8p[5/2]_3$	3353.26 [L2228]
3365.674(16)	8.37×10^4	4.12	0.057(14)	$4f[9/2]_5-8d[7/2]_4$	
3371.807(8)	6.89×10^5	6.19	0.061(6)	$6d[3/2]_1-5f[5/2]_2$	3371.81 [L2228]
3383.723(19)	4.68×10^4	4.57	0.045(18)	$7p[3/2]_1-7d[1/2]_1$	3383.73 [L2228]
3394.885(14)	7.70×10^5	5.25	0.085(13)	$7p[5/2]_2-5d'[5/2]_3$	3394.88 [L2228]
3402.246(9)	1.39×10^6	5.41	0.079(6)	$7s[3/2]_1-7p[1/2]_0$	3402.24 [L2228]
3441.791(18)	2.96×10^5	5.28	0.083(16)	$7p[3/2]_2-7d[1/2]_1$	3441.78 [L2228]
3497.723(7)	5.34×10^6	6.23	0.068(5)	$7s[3/2]_2-7p[3/2]_2$	3497.73 [L2228]
3520.353(4)	2.33×10^{-2}	11.5	0.024(3)	$7p[1/2]_1-5d'[3/2]_2$	
3522.456(2)	4.63×10^{-1}	10.2	0.037(3)	$6p[5/2]_3-5d[5/2]_2$	3522.45 [L2228]
3555.785(3)	5.02×10^{-2}	16.0	0.031(3)	$7s[3/2]_2-7p[3/2]_1$	3555.78 [L2228]
3559.182(6)	2.09×10^{-2}	6.59	0.030(6)	$6p'[3/2]_2-7d[3/2]_2$	3559.17 [L2228]
3603.506(10)	2.31×10^{-2}	5.53	0.060(9)	$6d[1/2]_1-8p[1/2]_1$	3603.50 [L2228]
3662.273(16)	1.50×10^{-2}	2.41	0.062(13)	$6d[1/2]_0-8p[1/2]_1$	3662.36 [L2228]
3662.462(78)	3.18×10^{-2}	6.66	0.032(78)	$6d[3/2]_2-8p[3/2]_2$	3662.36 [L2228]
3758.217(5)	6.80×10^{-2}	6.40	0.051(4)	$6p'[1/2]_0-5d'[3/2]_1$	3758.23 [L2228]
3771.013(3)	9.47	6.60	0.035(3)	$6p[1/2]_0-5d[3/2]_1$	3771.07(11) [L7449]
3805.719(2)	7.36	13.4	0.041(3)	$6p[5/2]_2-5d[5/2]_2$	3805.77(12) [L7449]
3838.690(5)	2.38×10^{-2}	6.10	0.025(5)	$7s[3/2]_1-6p'[1/2]_1$	3838.68 [L2228]
3841.720(5)	1.11×10^{-1}	3.86	0.029(2)	$4f[7/2]_4-6g[9/2]_5$	
3841.801(6)	1.01×10^{-1}	3.20	0.030(2)	$4f[7/2]_3-6g[9/2]_4$	
3866.897(7)	2.18×10^{-2}	5.78	0.044(6)	$6d[5/2]_3-5f[5/2]_3$	
3871.785(6)	2.40×10^{-2}	8.19	0.030(5)	$7p[1/2]_0-7d[3/2]_1$	3871.78 [L2228]
3872.167(2)	1.07×10^{-1}	28.1	0.029(2)	$4f[5/2]_2-6g[7/2]_3$	
3875.125(2)	1.07×10^{-1}	26.5	0.030(2)	$4f[5/2]_3-6g[7/2]_4$	
3886.331(2)	9.61×10^{-2}	23.4	0.030(2)	$6d[5/2]_3-5f[7/2]_4$	
3913.528(2)	1.33×10^{-1}	24.6	0.031(2)	$4f[9/2]_4-6g[11/2]_5$	
3914.381(2)	1.58×10^{-1}	22.7	0.031(2)	$4f[9/2]_5-6g[11/2]_6$	
3922.154(3)	1.22×10^{-1}	6.35	0.030(2)	$4f[3/2]_2-6g[5/2]_3$	
3931.750(4)	5.77×10^{-2}	9.80	0.035(3)	$4f[3/2]_1-6g[5/2]_2$	
3933.967(7)	7.73×10^{-2}	7.41	0.050(6)	$7p[3/2]_1-7d[5/2]_2$	3933.96 [L2228]
3959.631(6)	3.23×10^{-2}	8.64	0.035(5)	$7p[3/2]_2-7d[7/2]_3$	
3969.489(8)	3.99×10^{-2}	11.1	0.056(8)	$7p[3/2]_2-7d[3/2]_1$	
3973.579(13)	7.30×10^{-2}	8.61	0.072(13)	$7s[3/2]_2-6p[3/2]_2$	3973.57 [L2228]
3975.719(2)	8.99×10^{-1}	12.3	0.029(2)	$7p[5/2]_3-7d[7/2]_4$	3975.70 [L2228]
3992.017(8)	3.04×10^{-2}	7.26	0.050(8)	$7p[3/2]_2-7d[5/2]_2$	
4027.147(2)	4.27	12.4	0.043(2)	$6p[5/2]_3-5d[5/2]_3$	4027.03(13) [L7449]
4035.039(3)	5.35×10^{-2}	12.6	0.038(3)	$7p[3/2]_2-7d[3/2]_2$	
4047.106(2)	2.67×10^{-1}	12.8	0.031(2)	$7p[3/2]_2-7d[5/2]_3$	
4089.932(4)	1.36×10^{-1}	12.7	0.028(4)	$7s[3/2]_2-6p'[1/2]_1$	
4177.554(7)	1.05×10^5	7.16	0.053(14)	$6d[5/2]_2-7f[7/2]_3$	
4201.157(7)	2.96×10^5	5.43	0.074(10)	$7p[1/2]_1-7d[1/2]_1$	
4264.391(5)	2.71×10^5	10.1	0.053(8)	$7p[5/2]_3-7d[5/2]_3$	
4294.448(5)	1.72×10^6	10.8	0.059(5)	$7p[5/2]_2-7d[7/2]_3$	
4299.395(6)	1.29×10^5	7.62	0.040(13)	$6p'[3/2]_1-7d[5/2]_2$	
4310.411(5)	3.80×10^7	8.47	0.070(6)	$6p[5/2]_2-5d[5/2]_3$	4310.72(15) [L7449]
4332.803(7)	4.39×10^5	5.24	0.078(10)	$7p[1/2]_1-7d[1/2]_0$	
4342.416(7)	9.09×10^4	5.36	0.054(17)	$6p'[3/2]_1-7d[3/2]_2$	
4353.305(5)	4.22×10^5	6.84	0.061(6)	$6d[7/2]_3-5f[9/2]_4$	
4369.858(5)	1.28×10^5	7.55	0.060(10)	$7p[5/2]_2-7d[3/2]_2$	
4420.004(7)	7.16×10^5	5.18	0.082(7)	$7s[3/2]_1-6p'[1/2]_0$	
4461.704(7)	1.00×10^6	6.40	0.104(20)	$5d[3/2]_1-7p[5/2]_2$	
4465.781(5)	4.26×10^5	7.04	0.060(7)	$6d[7/2]_4-5f[9/2]_5$	
4489.155(6)	1.22×10^5	5.06	0.046(15)	$5d[3/2]_1-6p'[3/2]_1$	
4656.368(5)	9.41×10^6	7.45	0.057(7)	$6p[1/2]_1-5d[5/2]_2$	4656.369(3) [L9760]
4677.513(7)	9.85×10^5	5.82	0.105(9)	$6p[3/2]_1-5d[3/2]_1$	4677.511(3) [L9760]
4693.006(8)	4.93×10^4	3.88	0.045(24)	$6d[3/2]_1-5f[5/2]_3$	
4711.752(8)	4.08×10^4	4.75	0.036(20)	$7p[3/2]_2-9s[3/2]_2$	
4727.762(13)	5.61×10^4	3.72	0.084(43)	$6d[3/2]_1-6f[5/2]_2$	
4735.620(11)	2.57×10^4	3.34	0.041(27)	$7p[3/2]_2-9s[3/2]_1$	
4751.401(6)	8.79×10^4	6.53	0.050(12)	$7p[1/2]_1-7d[5/2]_2$	
4786.940(8)	4.02×10^4	4.84	0.044(24)	$7p[1/2]_1-7d[3/2]_1$	
4794.401(7)	1.16×10^5	5.72	0.048(15)	$7p[1/2]_1-7d[3/2]_2$	4794.412(3) [L9760]
4796.535(7)	1.90×10^5	5.46	0.111(18)	$5d[3/2]_1-7p[3/2]_2$	4796.529(3) [L9760]
4854.596(8)	8.34×10^4	3.51	0.061(25)	$5d[3/2]_1-7p[3/2]_1$	4854.583(3) [L9760]
4929.037(5)	1.24×10^5	9.90	0.038(9)	$7p[5/2]_1-9s[3/2]_2$	4929.029(3) [L9760]
4933.945(6)	3.12×10^7	6.77	0.091(4)	$6p[3/2]_1-5d[3/2]_1$	4933.941(3) [L9760]
4952.284(5)	8.94×10^5	6.66	0.064(6)	$5d[3/2]_1-7p[1/2]_0$	4952.282(3) [L9760]
5234.924(12)	1.01×10^{-3}	3.97	0.115(25)	$6d[5/2]_1-6f[7/2]_4$	
5321.046(10)	4.00×10^{-2}	4.73	0.116(13)	$6p[1/2]_0-7s[3/2]_1$	5321.052(3) [L9760]
5471.083(13)	8.53×10^{-4}	3.95	0.093(41)	$7p[1/2]_1-9s[3/2]_2$	5471.097(3) [L9760]
5526.222(21)	8.78×10^{-4}	2.32	0.143(57)	$6d[5/2]_2-6f[7/2]_3$	

(continued on next page)

Table 2 (continued).

ν_{ki} (cm ⁻¹)	I_{ki} (arb. u.)	SNR	FWHM (cm ⁻¹)	Identification	Other work (if any)
5683.494(11)	1.98×10^{-3}	4.40	0.122(15)	$7p[3/2]_2-8d[5/2]_3$	
5718.328(13)	3.04×10^{-3}	4.01	0.127(21)	$7s[3/2]_2-4f[5/2]_3$	5718.290(3) [L9760]
5719.819(18)	5.37×10^{-4}	2.30	0.088(65)	$6d[7/2]_3-6f[9/2]_4$	
5757.103(17)	4.81×10^{-3}	2.82	0.113(21)	$7p[5/2]_2-8d[7/2]_4$	5757.099(3) [L9760]
5770.171(23)	2.30×10^{-1}	2.29	0.164(18)	$6p[5/2]_2-5d[3/2]_1$	5770.164(3) [L9760]
5921.449(17)	2.47×10^{-3}	2.84	0.122(22)	$5d[5/2]_3-7p[5/2]_2$	5921.473(3) [L9760]
5938.536(15)	2.72×10^{-3}	2.96	0.107(27)	$7p[5/2]_2-8d[7/2]_3$	
5970.042(16)	4.31×10^{-3}	2.82	0.111(20)	$5d[3/2]_1-6p'[1/2]_0$	5970.044(3) [L9760]
5976.307(17)	2.19×10^{-1}	2.69	0.126(17)	$6p[3/2]_2-7s[3/2]_2$	5976.312(3) [L9760]
6039.003(17)	1.08×10^{-2}	2.87	0.123(18)	$5d[5/2]_3-7p[5/2]_3$	6039.1 [L2228]
6227.548(10)	1.07×10^{-1}	4.86	0.108(13)	$6p[3/2]_2-7s[3/2]_1$	6228.04(4) [L7384]
6232.739(10)	7.11×10^{-3}	4.88	0.110(14)	$6p[3/2]_1-7s[3/2]_2$	6232.7 [L2228]
6256.296(9)	2.65×10^{-2}	4.99	0.104(14)	$5d[5/2]_3-7p[3/2]_2$	6256.3 [L2228]
6300.867(15)	1.25×10^{-3}	3.45	0.133(47)	$7p[1/2]_1-8d[1/2]_1$	6300.9 [L2228]
6358.535(18)	1.19×10^{-3}	2.69	0.120(34)	$7p[1/2]_1-8d[3/2]_2$	6358.5 [L2228]
6426.163(7)	1.14×10^{-2}	8.01	0.107(11)	$5d[5/2]_2-7p[5/2]_2$	6426.2 [L2228]
6442.252(16)	1.38×10^{-3}	2.88	0.117(26)	$6p'[1/2]_1-7s'[1/2]_0$	6442.2 [L2228]
6453.600(18)	2.37×10^{-3}	2.86	0.141(24)	$5d[5/2]_2-6p'[3/2]_1$	6453.6 [L2228]
6483.980(10)	2.86×10^{-1}	4.86	0.113(12)	$6p[3/2]_1-7s[3/2]_1$	
6620.809(11)	6.92×10^{-3}	4.62	0.118(16)	$6p[1/2]_1-5d[3/2]_1$	6620.8 [L2228]
6638.219(10)	2.26×10^{-3}	4.84	0.100(19)	$6p'[3/2]_2-7s'[1/2]_1$	6638.2 [L2228]
6732.171(9)	1.27×10^{-3}	5.94	0.118(22)	$5d[5/2]_3-6p'[3/2]_2$	6732.2 [L2228]
6780.727(16)	1.13×10^{-3}	2.72	0.100(44)	$7p[5/2]_2-9d[7/2]_4$	
6785.712(10)	5.99×10^{-1}	4.61	0.111(13)	$6p[5/2]_3-7s[3/2]_2$	
6819.040(11)	1.10×10^{-2}	4.34	0.116(16)	$5d[5/2]_2-7p[3/2]_1$	6819.49(4) [L7384]
6893.070(17)	1.44×10^{-3}	2.69	0.111(41)	$7s[3/2]_1-8p[3/2]_1$	6893.0 [L2228]
6930.930(17)	1.00×10^{-3}	2.82	0.120(34)	$7s[3/2]_1-8p[3/2]_2$	6930.9 [L2228]
6949.801(10)	1.85×10^{-3}	4.95	0.110(16)	$5d[3/2]_1-4f[3/2]_1$	6949.9(2) [L4085]
6959.464(9)	3.30×10^{-2}	5.28	0.106(12)	$5d[3/2]_1-4f[3/2]_2$	6959.51(4) [L7384]
6964.499(22)	1.89×10^{-3}	2.33	0.160(29)	$7s[3/2]_2-8p[1/2]_1$	6964.5 [L4211c2]
7020.076(11)	6.67×10^{-2}	4.40	0.112(14)	$5d[3/2]_1-4f[5/2]_2$	7019.87(4) [L7384]
7032.596(17)	5.97×10^{-4}	2.77	0.108(45)	$7s[3/2]_2-8p[5/2]_2$	7032.6 [L2228]
7068.974(15)	1.29×10^{-1}	3.10	0.119(14)	$6p[5/2]_2-7s[3/2]_2$	
7076.169(15)	4.10×10^{-3}	3.00	0.111(17)	$7s[3/2]_2-8p[5/2]_3$	7076.2 [L2228]
7115.084(17)	1.11×10^{-3}	2.69	0.106(45)	$7s[3/2]_1-8p[1/2]_0$	7115.1 [L2228]
7320.216(14)	2.71×10^{-1}	3.32	0.116(14)	$6p[5/2]_2-7s[3/2]_1$	
7381.240(15)	2.49×10^{-2}	3.17	0.113(17)	$5d[7/2]_3-7p[5/2]_2$	7381.242 [L2228]
7498.767(10)	3.04×10^{-3}	4.78	0.101(18)	$5d[7/2]_3-7p[5/2]_3$	7498.8 [L2228]
8056.377(5)	5.53×10^{-5}	10.1	0.032(5)	$5d[3/2]_2-6p'[13/2]_1$	8056.4 [L2228]
8155.863(5)	1.74×10^{-3}	21.8	0.045(3)	$5d[1/2]_0-7p[1/2]_1$	8155.832(20) [L7293]
8170.870(5)	1.38×10^{-2}	23.5	0.042(3)	$6p[1/2]_1-7s[3/2]_1$	8170.877(20) [L7293]
8191.910(15)	4.29×10^{-4}	6.29	0.060(14)	$5d[7/2]_3-6p'[3/2]_2$	8192.1(2) [L4085]
8272.585(5)	4.51×10^{-3}	13.3	0.038(3)	$5d[7/2]_4-7p[5/2]_3$	8272.594(21) [L7293]
8363.754(5)	2.88×10^{-3}	37.8	0.054(3)	$5d[3/2]_2-7p[3/2]_2$	8363.812(21) [L7293]
8365.065(8)	3.27×10^{-4}	9.26	0.038(7)	$5d[1/2]_1-7p[5/2]_2$	8365.14(7) [L7293]
8392.509(6)	1.06×10^{-3}	18.5	0.046(4)	$5d[1/2]_1-6p'[3/2]_1$	8392.528(21) [L7293]
8419.243(16)	3.49×10^{-4}	5.53	0.052(14)	$5d[5/2]_3-4f[3/2]_2$	8419.202(21) [L7293]
8430.813(5)	2.20×10^{-3}	18.6	0.036(3)	$6p[1/2]_0-6d[1/2]_1$	8430.917(21) [L7293]
8431.302(7)	5.01×10^{-3}	5.72	0.047(4)	$5d[5/2]_3-4f[9/2]_4$	8431.308(21) [L7293]
8476.895(8)	6.07×10^{-3}	14.8	0.052(6)	$5d[5/2]_3-4f[5/2]_3$	8476.884(22) [L7293]
8513.926(5)	2.87×10^{-2}	18.9	0.039(2)	$5d[5/2]_3-4f[7/2]_4$	8513.935(6) [L9760]
8607.857(8)	3.55×10^{-3}	13.1	0.065(6)	$5d[1/2]_0-6p'[3/2]_1$	8607.882(22) [L7293]
8699.883(5)	1.48×10^{-3}	23.4	0.044(3)	$5d[1/2]_1-7p[3/2]_2$	8699.914(23) [L7293]
8757.944(6)	1.24×10^{-3}	19.3	0.043(3)	$5d[1/2]_1-7p[3/2]_1$	8757.974(23) [L7293]
8855.646(8)	7.24×10^{-3}	11.9	0.060(7)	$5d[1/2]_1-7p[1/2]_0$	8855.677(24) [L7293]
8973.292(7)	1.84×10^{-3}	15.2	0.075(5)	$5d[1/2]_0-7p[3/2]_1$	8973.281(3) [L9760]
8984.540(5)	4.19×10^{-3}	15.2	0.058(3)	$5d[5/2]_2-4f[5/2]_2$	8984.535(3) [L9760]
9018.541(5)	1.91×10^{-2}	16.5	0.046(3)	$5d[5/2]_2-4f[7/2]_3$	9018.537(3) [L9760]
9175.738(7)	1.06×10^{-2}	15.0	0.065(4)	$5d[1/2]_1-6p'[3/2]_2$	9175.736(3) [L9760]
9223.986(5)	2.41×10^{-1}	26.0	0.063(3)	$6s[3/2]_1-6p[1/2]_1$	9223.98(2) [L7293]
9292.091(9)	2.23×10^{-3}	12.5	0.053(8)	$5d[1/2]_1-6p'[1/2]_1$	9292.12(2) [L7293]
9337.317(20)	7.05×10^{-3}	25.8	0.056(2)	$6p[3/2]_2-6d[1/2]_1$	9337.32(2) [L7293]
9476.289(27)	3.47×10^{-4}	3.94	0.079(26)	$5d[3/2]_1-5f[3/2]_2$	9476.29(3) [L7293]
9496.002(5)	2.45×10^{-2}	16.6	0.057(2)	$6p[3/2]_2-6d[3/2]_2$	9496.007(6) [L9760]
9507.444(6)	4.44×10^{-3}	11.9	0.062(3)	$5d[1/2]_0-6p'[1/2]_1$	9507.483(21) [L4739]
9514.000(10)	6.59×10^{-4}	9.20	0.067(9)	$5d[3/2]_1-5f[5/2]_2$	9514.033(21) [L4739]
9534.999(8)	6.66×10^{-4}	10.5	0.045(7)	$6p[3/2]_1-6d[1/2]_0$	9534.976(21) [L4739]
9752.440(5)	4.04×10^{-3}	20.1	0.052(2)	$6p[3/2]_1-6d[3/2]_2$	9752.406(22) [L4739]
9812.430(8)	5.87×10^{-4}	11.1	0.045(7)	$6p[3/2]_2-6d[7/2]_3$	9812.433(22) [L4739]
9873.403(8)	2.36×10^{-3}	9.21	0.072(6)	$5d[1/2]_1-6p'[1/2]_0$	9873.378(22) [L4739]
9891.065(5)	1.66×10^{-2}	40.3	0.042(2)	$5d[7/2]_3-4f[9/2]_4$	9891.089(23) [L4739]
9913.194(5)	2.20×10^{-3}	18.8	0.044(3)	$6p[1/2]_0-6d[3/2]_1$	9913.205(23) [L4739]
9973.613(7)	2.43×10^{-3}	7.98	0.056(5)	$5d[7/2]_3-4f[7/2]_3$	9973.602(23) [L4739]
9973.691(10)	1.91×10^{-3}	4.44	0.078(7)	$5d[7/2]_3-4f[7/2]_4$	9973.602(23) [L4739]

(continued on next page)

Table 2 (continued).

ν_{ki} (cm ⁻¹)	I_{ki} (arb. u.)	SNR	FWHM (cm ⁻¹)	Identification	Other work (if any)
10030.785(12)	1.21×10^{-4}	4.84	0.024(11)	$6p[3/2]_2-6d[5/2]_2$	10030.782(23) [L4739]
10074.645(7)	7.86×10^{-1}	7.00	0.110(3)	$6s[3/2]_1-6p[5/2]_2$	10074.6342(71) [L7292]
10201.602(14)	1.07	5.24	0.125(11)	$6s[3/2]_2-6p[1/2]_1$	10201.5997(21) [L7292]
10287.226(5)	9.00×10^{-3}	61.5	0.044(2)	$6p[3/2]_1-6d[5/2]_2$	10287.193(24) [L4739]
10305.415(8)	8.08×10^{-4}	11.6	0.060(7)	$6p[5/2]_3-6d[3/2]_2$	10305.400(24) [L4739]
10322.102(5)	1.10×10^{-2}	13.3	0.045(2)	$6p[3/2]_2-6d[5/2]_3$	10322.073(25) [L4739]
10429.982(10)	6.76×10^{-4}	10.9	0.055(8)	$6p[5/2]_2-6d[1/2]_1$	10429.955(25) [L4739]
10508.628(5)	3.29×10^{-2}	20.0	0.043(2)	$6p[5/2]_3-6d[7/2]_4$	10508.6318(22) [L7292]
10526.696(6)	1.79×10^{-3}	20.3	0.055(4)	$5d[3/2]_2-4f[3/2]_2$	10526.676(25) [L4739]
10584.342(5)	6.11×10^{-3}	72.9	0.043(2)	$5d[3/2]_2-4f[5/2]_3$	10584.328(26) [L4739]
10587.308(14)	3.19×10^{-4}	5.64	0.048(12)	$5d[3/2]_2-4f[5/2]_2$	10587.309(26) [L4739]
10588.686(20)	3.82×10^{-4}	4.92	0.069(19)	$6p[5/2]_2-6d[3/2]_2$	10588.677(26) [L4739]
10621.828(5)	3.61×10^{-3}	53.6	0.042(2)	$6p[5/2]_3-6d[7/2]_3$	10621.809(26) [L4739]
10664.024(5)	1.30×10^{-2}	17.6	0.044(2)	$5d[7/2]_4-4f[9/2]_1$	10664.014(26) [L4739]
10664.880(14)	3.14×10^{-4}	5.71	0.039(12)	$5d[7/2]_4-4f[9/2]_4$	10664.856(27) [L4739]
10742.100(11)	2.07×10^{-3}	13.5	0.120(10)	$6s'[1/2]_1-7p[1/2]_1$	10742.069(27) [L4739]
10747.508(6)	1.29×10^{-3}	22.2	0.051(4)	$5d[7/2]_4-4f[7/2]_4$	10747.485(27) [L4739]
10840.189(12)	1.69×10^{-4}	5.14	0.034(10)	$6p[5/2]_3-6d[5/2]_2$	10840.201(27) [L4739]
10853.160(8)	6.83×10^{-4}	10.1	0.051(7)	$5d[1/2]_1-4f[3/2]_1$	10853.158(27) [L4739]
10862.829(9)	1.37×10^{-3}	11.1	0.075(7)	$5d[1/2]_1-4f[3/2]_2$	10862.805(27) [L4739]
10905.083(5)	1.22×10^{-2}	28.4	0.045(2)	$6p[5/2]_2-6d[7/2]_3$	10905.083(27) [L4739]
10910.879(6)	2.88×10^{-1}	8.44	0.096(2)	$6s[3/2]_1-6p[3/2]_1$	10910.8763(6) [L7292]
10923.427(18)	4.18×10^{-4}	5.58	0.073(16)	$5d[1/2]_1-4f[5/2]_2$	10923.432(27) [L4739]
10990.697(10)	5.35×10^{-4}	8.76	0.050(8)	$5d[5/2]_3-5f[7/2]_4$	10990.670(28) [L4739]
11052.253(5)	2.41×10^{-1}	20.4	0.080(3)	$6s[3/2]_2-6p[5/2]_2$	11052.2523(6) [L7292]
11068.504(7)	7.85×10^{-4}	12.1	0.053(5)	$5d[1/2]_0-4f[3/2]_1$	11068.486(28) [L4739]
11076.129(13)	4.83×10^{-4}	6.92	0.065(11)	$6p[3/2]_1-6d[3/2]_1$	11076.089(28) [L4739]
11123.463(5)	2.07×10^{-3}	23.7	0.051(3)	$6p[5/2]_2-6d[5/2]_2$	11123.424(12) [L4739]
11131.506(8)	8.63×10^{-4}	11.3	0.052(7)	$6p[5/2]_3-6d[5/2]_3$	11131.500(21) [L4739]
11166.637(23)	2.87×10^{-4}	2.66	0.038(22)	$6s'[1/2]_1-7p[5/2]_2$	11166.649(21) [L4739]
11167.310(5)	1.34×10^{-1}	16.3	0.076(3)	$6s[3/2]_1-6p[3/2]_2$	11167.3092(6) [L7292]
11194.087(5)	3.02×10^{-3}	21.1	0.059(3)	$6s'[1/2]_1-6p'[3/2]_1$	11194.094(21) [L4739]
11221.880(5)	2.69×10^{-3}	29.4	0.053(3)	$6p[1/2]_1-6d[1/2]_0$	11221.863(21) [L4739]
11280.634(5)	5.50×10^{-3}	22.8	0.057(2)	$6p[1/2]_1-6d[1/2]_1$	11280.630(22) [L4739]
11335.520(11)	4.16×10^{-1}	6.42	0.122(9)	$6s[3/2]_2-6p[5/2]_3$	11335.5135(6) [L7292]
11414.773(11)	4.99×10^{-4}	5.97	0.054(10)	$6p[5/2]_2-6d[5/2]_3$	11414.736(22) [L4739]
11439.323(5)	2.89×10^{-3}	11.6	0.055(2)	$6p[1/2]_1-6d[3/2]_2$	11439.328(3) [L7292]
11475.949(7)	2.72×10^{-4}	10.4	0.025(5)	$5d[5/2]_2-5f[5/2]_3$	11475.875(22) [L4739]
11495.307(11)	3.22×10^{-4}	7.21	0.041(9)	$5d[5/2]_2-5f[7/2]_3$	11495.246(22) [L4739]
11888.488(7)	1.79×10^{-2}	13.7	0.081(5)	$6s[3/2]_2-6p[3/2]_1$	11888.4857(7) [L7292]
11977.314(5)	6.10×10^{-3}	60.2	0.058(3)	$6s'[1/2]_1-6p'[3/2]_2$	11977.3164(7) [L7292]
12073.808(7)	7.75×10^{-2}	6.03	0.080(2)	$6s[3/2]_1-6p[1/2]_0$	12073.8065(7) [L7292]
12093.667(13)	7.64×10^{-4}	6.79	0.057(12)	$6s'[1/2]_1-6p'[1/2]_1$	12093.665(3) [L7292]
12144.927(7)	1.65×10^{-1}	30.4	0.115(5)	$6s[3/2]_2-6p[3/2]_2$	12144.9184(7) [L7292]
12182.349(9)	1.58×10^{-3}	9.82	0.081(8)	$6s'[1/2]_0-6p'[3/2]_1$	12182.357(3) [L7292]
12407.745(21)	3.95×10^{-4}	5.01	0.070(19)	$5d[7/2]_3-5f[9/2]_4$	12407.758(3) [L7292]

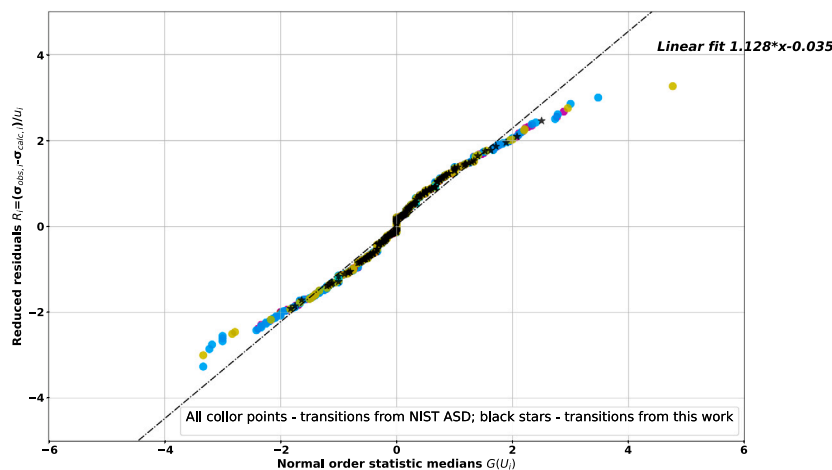


Fig. 5. Normal probability plot of reduced residuals from two datasets: (i) all dipole-allowed transitions listed at NIST database [11] and (ii) our linelist. The most of both data points align relatively close to the straight line with a unit slope. This implies that our R_i values exhibit a distribution close to the normal distribution.

n , which is whole amount of used transitions. For the measurements to be consistent with the given identifications it would be expected that

the root mean square (RMS) value of the R_i values is close to or less than 1. Generated normal probability plot on Fig. 5 shows that R_i values

Table 3

Refinement of Xe 6 g, 6h, 7h, 7i levels. The complete list of re-optimized levels with uncertainties and comparison with the NIST ASD [11] values is included as a supplementary online material.

Level	Energy (cm ⁻¹)
7i $\left[\frac{9}{2} \right]_5$	95592.28(5)
7i $\left[\frac{9}{2} \right]_4$	95592.29(7)
7i $\left[\frac{15}{2} \right]_8$	95592.82(4)
7i $\left[\frac{15}{2} \right]_7$	95592.82(5)
7i $\left[\frac{11}{2} \right]_6$	95594.515(20)
7i $\left[\frac{11}{2} \right]_5$	95594.524(24)
7i $\left[\frac{13}{2} \right]_7$	95594.99(3)
7i $\left[\frac{13}{2} \right]_6$	95595.00(4)
7h $\left[\frac{7}{2} \right]_3$	95590.33(6)
7h $\left[\frac{7}{2} \right]_4$	95590.39(5)
7h $\left[\frac{13}{2} \right]_7$	95591.382(18)
7h $\left[\frac{13}{2} \right]_6$	95591.384(20)
7h $\left[\frac{9}{2} \right]_5$	95594.068(28)
7h $\left[\frac{9}{2} \right]_4$	95594.077(31)
6h $\left[\frac{7}{2} \right]_4$	94779.573(10)
6h $\left[\frac{7}{2} \right]_3$	94779.584(11)
6h $\left[\frac{13}{2} \right]_7$	94781.219(15)
6h $\left[\frac{13}{2} \right]_6$	94781.221(13)
6h $\left[\frac{9}{2} \right]_5$	94785.474(12)
6h $\left[\frac{9}{2} \right]_4$	94785.483(14)
6h $\left[\frac{11}{2} \right]_6$	94787.096(12)
6h $\left[\frac{11}{2} \right]_5$	94787.106(17)
6g $\left[\frac{5}{2} \right]_2$	94771.528(6)
6g $\left[\frac{5}{2} \right]_3$	94771.593(5)
6g $\left[\frac{11}{2} \right]_6$	94775.0312(49)
6g $\left[\frac{11}{2} \right]_5$	94775.0337(48)
6g $\left[\frac{7}{2} \right]_4$	94782.2095(52)
6g $\left[\frac{7}{2} \right]_3$	94782.222(4)
6g $\left[\frac{9}{2} \right]_4$	94785.845(6)
6g $\left[\frac{9}{2} \right]_5$	94785.852(6)

are close to the normal statistical distribution (slope is 1.13, the vertical offset from the origin is 0.04).

When generating the normal probability plot in Fig. 5, we excluded the lines that solely determine one of the levels. We also excluded duplicate lines measured in different studies, selecting the value with the smaller uncertainty. It should also be noted that we used revised estimates of uncertainties for many of the NIST ASD lines, most notably Humphreys and Meggers [6], Humphreys and Kostkowski [7], Mishra et al. [9]. The supplementary table with the full line list (LOPT input file) contain these revised uncertainties.

The distribution of the residuals R_i , shows that the system of Xe I levels obtained in our optimization procedure is internally consistent within ≈ 0.02 cm⁻¹. The resulting complete list of re-optimized levels (actually, the LOPT level output file) with uncertainties and comparison with the NIST ASD [11] values is included as a supplementary online material. Table 3 contains newly reported Rydberg levels that belong to

the 6 g, 6 h, 7 h, 7i configurations only. Unfortunately, we were unable to resolve all components of the 7 h multiplet. The reason is probably that the transitions involving 7h[11/2] are weak and/or blended by other multiplet components. As a result, only 6 out of 8 lines of the 7 h multiplet are included in Table 3.

LOPT code is able to return different values of level uncertainties [38, Eqs. (26), (31), (32)]. The uncertainty D_2 relative to the ground level, is frequently used. However, in rare gases the excited levels are usually measured much more accurately relative to the lowest excited level in this case, 6s[3/2]₂. Thus, all uncertainties (including the ground level) specified in Table 3 are given for the intervals from this base level. The uncertainties of excitation energies from the ground level must be calculated as sums in quadrature of the tabulated uncertainty and that of the ground level (0.004 cm⁻¹ in this case).

4. Conclusion

Although the neutral xenon (Xe I) spectra have been studied for a long time, an important part of mid-infrared (MIR) spectral region has not been studied in precision laboratory measurements. As a result, no high-quality spectroscopic data for Xe I are available in the literature (for instance, the NIST ASD [11] lacks experimental lines with wavenumbers less than 1800 cm⁻¹). However, this spectral range can be of interest for infrared astronomy as well as for infrared lasing [47, 48]; therefore, providing new spectroscopic data for Xe in the infrared domain is important.

This study attempts to fill the gap in the high-resolution MIR spectra of Xe I. Most of the Xe I spectrum measurements were performed more than a half century ago. In this study, we remeasured the Xe I emission spectrum within the wavelength range of 0.7–14 μm (corresponding to the wavenumber range of 700–14,000 cm⁻¹). 335 lines of atomic xenon are reported, and 111 of them are observed for the first time. No high-resolution spectra have previously been available for the spectral region below 2000 cm⁻¹ (wavelength longer than 5 μm). The most prominent lines in this region are due, as a rule, to transitions from Rydberg levels with high orbital momentum, $l = 4..6$ (g-, h-, and i-levels). After combining all available Xe I lines in a least-square optimization procedure, we have obtained an updated Xe I level system, which now includes the newly observed Rydberg 6 g, 6 h, 7 h, and 7i levels. Our improved system of Xe I levels is internally consistent within ≈ 0.02 cm⁻¹.

CRediT authorship contribution statement

S. Civiš: Supervision, Resources, Project administration, Methodology, Formal analysis, Data curation, Conceptualization. **E.M. Zanoina:** Writing – review & editing, Writing – original draft, Visualization, Validation, Formal analysis, Data curation. **P. Kubelík:** Validation, Software, Resources, Project administration, Methodology, Formal analysis, Data curation. **V.E. Chernov:** Writing – review & editing, Writing – original draft, Supervision, Formal analysis. **A. Pastorek:** Formal analysis, Data curation. **M. Ferus:** Supervision, Project administration, Funding acquisition.

Declaration of competing interest

The authors declare that they have no known competing financial interests or personal relationships that could have appeared to influence the work reported in this paper.

Data availability

Data will be made available on request.

Acknowledgments

We wish to thank Alexander E. Kramida from National Institute of Standards and Technology for helpful recommendations and advices on processing all data for our compilation, which significantly enhanced the accuracy and reliability of our work.

This work was supported by the ERDF/ESF “Centre of Advanced Applied Sciences” (no. CZ.02.1.01/0.0/0.0/16_019/0000778) (S.C.). P.K. acknowledges the support from the Czech Science Foundation (grant no. 20-10591J). V.Ch. acknowledges the support from the Ministry of Science and Higher Education of Russian Federation (grant number FZGU-2020-0035).

Appendix A. Supplementary data

Supplementary material related to this article can be found online at <https://doi.org/10.1016/j.jqsrt.2024.108939>.

References

- [1] Abbink JH, Dorgelo HB. The krypton and xenon spectrum in the extreme ultraviolet. *Z Phys* 1928;47(3-4):221–32. <http://dx.doi.org/10.1007/BF02055797>.
- [2] Meggers W, deBruin T, Humphreys C. The first spectrum of xenon. *Bur Stand J Res* 1929;3(4/6):731–63.
- [3] Humphreys CJ. Interference measurements in the first spectra of krypton and xenon. *Bur Stand J Res* 1930;5(5):1041–55. <http://dx.doi.org/10.6028/jres.005.063>.
- [4] Meggers WF, Humphreys CJ. Interference measurements in the spectra of noble gases. *J Res Nat Bur Stand* 1934;13(3):293–309. <http://dx.doi.org/10.6028/jres.013.022>.
- [5] Meggers WF. Infrared spectra of noble gases (10500 to 13000 Å). *J Res Nat Bur Stand* 1935;14(RP781):487–97. <http://dx.doi.org/10.6028/jres.014.025>.
- [6] Humphreys CJ, Meggers WF. Further description and analysis of the first spectrum of xenon. *Bur Stand J Res* 1933;10(139–149). <http://dx.doi.org/10.6028/jres.010.012>.
- [7] Humphreys CJ, Kostkowski HJ. Infrared spectra of noble gases (12000 to 19000 Å). *J Res Nat Bur Stand* 1952;49(2):73–84. <http://dx.doi.org/10.6028/jres.049.010>.
- [8] Humphreys CJ. First spectra of neon, argon, and xenon 136 in the 1.2–4.0 μm region. *J Phys Chem Ref Data* 1973;2:519–30. <http://dx.doi.org/10.1063/1.3253126>.
- [9] Mishra AP, Kshirsagar RJ, Bellary VP, Balasubramanian TK. Identification of new transitions in the first spectra of neon, krypton and xenon in the near infrared by Fourier transform spectroscopy. *J Quant Spectrosc Radiat Transfer* 2000;67(1):1–7. [http://dx.doi.org/10.1016/S0022-4073\(99\)00189-2](http://dx.doi.org/10.1016/S0022-4073(99)00189-2).
- [10] Saloman EB. Energy levels and observed spectral lines of xenon, Xe I through Xe LIV. *J Phys Chem Ref Data* 2004;33(3):765–921. <http://dx.doi.org/10.1063/1.1649348>.
- [11] Kramida A, Ralchenko Y, Reader J, NIST ASD Team. NIST atomic spectra database (version 5.10). 2022, <http://dx.doi.org/10.18434/T4W30F>, URL <http://physics.nist.gov/asd>.
- [12] Kubelík P, Čiviš S, Pastorek A, Zanozina EM, Chernov VE, Juha L, et al. FTIR laboratory measurement of Ne I Rydberg states in 1.43–14.3 μm spectral range. *Astron Astrophys* 2015;582:A12. <http://dx.doi.org/10.1051/0004-6361/201526442>.
- [13] Kubelík P, Zanozina EM, Pastorek A, Ferus M, Juha L, Chernov VE, et al. Argon FTIR spectra between 800 and 2000 cm⁻¹: *h*- and *i*-levels and transition probabilities. *J Quant Spectrosc Radiat Transfer* 2016;182:337–45. <http://dx.doi.org/10.1016/j.jqsrt.2016.06.022>.
- [14] Čiviš S, Kubelík P, Pastorek A, Zanozina EM, Ferus M, Chernov VE, et al. Kr I spectra in the 5–14 μm range. *J Quant Spectrosc Radiat Transfer* 2020;249. <http://dx.doi.org/10.1016/j.jqsrt.2020.106985>, UNSP 106985.
- [15] Čiviš S, Kubelík P, Zanozina EM, Pastorek A, Chernov VE, Ferus M, et al. FTIR laboratory measurement of He I spectra in the 6.5–14 μm spectral range: Transitions involving *f*, *g*, *h*, and *i* states. *J Quant Spectrosc Radiat Transfer* 2021;262:107523. <http://dx.doi.org/10.1016/j.jqsrt.2021.107523>.
- [16] Brandi F, Velchev I, Hogervorst W, Ubachs W. Vacuum-ultraviolet spectroscopy of Xe: Hyperfine splittings, isotope shifts, and isotope-dependent ionization energies. *Phys Rev A* 2001;64(3):032505. <http://dx.doi.org/10.1103/PhysRevA.64.032505>.
- [17] Pawelec E, Mazouffre S, Sadeghi N. Hyperfine structure of some near-infrared Xe I and Xe II lines. *Spectrochim Acta, Part B* 2011;66(6):470–5. <http://dx.doi.org/10.1016/j.sab.2011.05.009>.
- [18] Bounds J, Kolomenskii A, Trainham R, Manard M, Schuessler H. Hyperfine structure and isotope shifts of xenon measured for near-infrared transitions with Doppler-free saturated absorption spectroscopy. *Spectrochim Acta, Part B* 2023;202:106635. <http://dx.doi.org/10.1016/j.sab.2023.106635>.
- [19] Ozawa A, Kobayashi Y. Vuv frequency-comb spectroscopy of atomic xenon. *Phys Rev A* 2013;87:022507. <http://dx.doi.org/10.1103/PhysRevA.87.022507>.
- [20] Kawaguchi K, Hama Y, Nishida S. Time-resolved Fourier transform infrared spectroscopy: Application to pulsed discharges. *J Mol Spectrosc* 2005;232(1):1–13. <http://dx.doi.org/10.1016/j.jms.2005.02.007>.
- [21] Čiviš S, Kubát P, Nishida S, Kawaguchi K. Time-resolved Fourier transform infrared emission spectroscopy of H₃⁺ molecular ion. *Chem Phys Lett* 2006;418(4–6):448–53. <http://dx.doi.org/10.1016/j.cplett.2005.10.136>.
- [22] Papoušek D, Ogilvie J, Čiviš S, Winnewisser M. The vibration-rotational bands v_3 , $2v_3 - v_3$, and $v_3 + v_6 - v_6$ of H₃¹²CF. *J Mol Spectrosc* 1991;149(1):109–24. [http://dx.doi.org/10.1016/0022-2852\(91\)90146-2](http://dx.doi.org/10.1016/0022-2852(91)90146-2).
- [23] Čiviš S, Szabla R, Szyja BM, Smykowski D, Ivanek O, Knížek A, et al. TiO₂-catalyzed synthesis of sugars from formaldehyde in extraterrestrial impacts on the early Earth. *Sci Rep* 2016;6:23199. <http://dx.doi.org/10.1038/srep23199>.
- [24] Kawaguchi K, Baskakov O, Hosaki Y, Hama Y, Kugimiya C. Time-resolved Fourier transform spectroscopy of pulsed discharge products. *Chem Phys Lett* 2003;369(3–4):293–8. [http://dx.doi.org/10.1016/S0009-2614\(02\)02017-1](http://dx.doi.org/10.1016/S0009-2614(02)02017-1).
- [25] Čiviš S, Kubelík P, Ferus M. Time-resolved Fourier transform emission spectroscopy of He/CH₄ in a positive column discharge. *J Phys Chem A* 2012;116(12):3137–47. <http://dx.doi.org/10.1021/jp211772d>, PMID: 22375598.
- [26] Čiviš S, Ferus M, Kubelík P, Jelfínek P, Zanozina EM, Chernov VE. Na I spectra in the 1.4–14 micron range: Transitions and oscillator strengths involving f, g, and h-states. *Astron Astrophys* 2012;542:A35. <http://dx.doi.org/10.1051/0004-6361/201219215>.
- [27] Čiviš S, Heays AN, Knížek A, Ferus M. High resolution emission FT spectra of sodium in a microwave discharge: Intensity variation of the D-1/D-2 lines in exoplanetary atmospheres. *J Quant Spectrosc Radiat Transfer* 2021;270. <http://dx.doi.org/10.1016/j.jqsrt.2021.107689>.
- [28] Gordon I, Rothman L, Hargreaves R, Hashemi R, Karlovets E, Skinner F, et al. The HITRAN2020 molecular spectroscopic database. *J Quant Spectrosc Radiat Transfer* 2022;277:107949. <http://dx.doi.org/10.1016/j.jqsrt.2021.107949>.
- [29] Rothman L, Gordon I, Barber R, Dothe H, Gamache R, Goldman A, et al. HITEMP, the high-temperature molecular spectroscopic database. *J Quant Spectrosc Radiat Transfer* 2010;111(15):2139–50. <http://dx.doi.org/10.1016/j.jqsrt.2010.05.001>, XVIth Symposium on High Resolution Molecular Spectroscopy (HighRus-2009).
- [30] Brault JW. High precision Fourier transform spectrometry: The critical role of phase corrections. *Microchim Acta* 1987;93(1):215–27. <http://dx.doi.org/10.1007/BF01201691>.
- [31] Martin W, Wiess W. Atomic, Molecular, and Optical Physics Handbook (version 2.2). Gaithersburg, MD, USA: National Institute of Standards and Technology; 2002, URL <https://www.nist.gov/pml/atomic-spectroscopy-compendium-basic-ideas-notations-data-and-formulas>.
- [32] Morillon C. Etude des spectres d'émission atomique du néon et du xénon entre 3,5 et 5,5 μm à l'aide d'un spectromètre à grilles. *Spectrochim. Acta, Part B* 1972;27(12):527–36. [http://dx.doi.org/10.1016/0584-8547\(72\)80052-1](http://dx.doi.org/10.1016/0584-8547(72)80052-1).
- [33] Humphreys CJ, Paul E, Cowan RD, Andrew KL. Spectra of the noble gases in the 4-μm region. *J Opt Soc Amer* 1967;57(7):855–64. <http://dx.doi.org/10.1364/JOSA.57.0000855>.
- [34] Faust WL, McFarlane RA, Patel CKN, Garrett CGB. Noble gas optical maser lines at wavelengths between 2 and 35 μ. *Phys Rev* 1964;133:A1476–86. <http://dx.doi.org/10.1103/PhysRev.133.A1476>.
- [35] Sittner WR, Peck ER. The spectra of argon, krypton, and xenon between 1.2 and 2.2 microns. *J Opt Soc Amer* 1949;39(6):474–7. <http://dx.doi.org/10.1364/JOSA.39.000474>.
- [36] Humphreys CJ, Paul J. Infrared atomic spectra. In: Quarterly report: foundational research projects. Corona, California: Naval Ordnance Laboratory; 1960, p. 23–40, NAVWEPS Report 5996.
- [37] Hepner G. Contribution à l'étude de l'émission infrarouge de spectres atomiques et moléculaires dans le domaine spectral 1-3 μ – application à l'élargissement des raies de la série de Paschen de l'atome d'hydrogène. *Ann. Phys. (Paris)* 1961;13(6):735–94. <http://dx.doi.org/10.1051/anphys/196113060735>.
- [38] Kramida AE. The program LOPT for least-squares optimization of energy levels. *Comput Phys Comm* 2011;182(2):419–34. <http://dx.doi.org/10.1016/j.cpc.2010.09.019>.
- [39] Labastie P, Biraben F, Giacobino E. Optogalvanic spectroscopy of the ns and nd Rydberg states of xenon. *J Phys B: At Mol Opt Phys* 1982;15(16):2595–603. <http://dx.doi.org/10.1088/0022-3700/15/16/010>.
- [40] Ahmed M, Baig M, Suleiman B. Laser optogalvanic spectroscopic studies of xenon. *J Phys B: At Mol Opt Phys* 1998;31(17):4017–28. <http://dx.doi.org/10.1088/0953-4075/31/17/021>.
- [41] Yoshino K, Freeman DE. Absorption spectrum of xenon in the vacuum-ultraviolet region. *J Opt Soc Amer B* 1985;2(8):1268–74. <http://dx.doi.org/10.1364/JOSAB.2.0001268>.
- [42] LHuillier A, Lompré L, Normand D, Morellec J, Ferray M, Lavancier J, et al. Spectroscopy of the np and nf even-parity Rydberg series in xenon by two-photon excitation. *J Phys B: At Mol Opt Phys* 1989;6(9):1644–7. <http://dx.doi.org/10.1088/0953-4075/6/9/001>.

- [43] Grandin J, Husson X. Even-parity Rydberg and auto-ionizing states in xenon. *J Phys B: At Mol Opt Phys* 1981;14(3):433–40. <http://dx.doi.org/10.1088/0022-3700/14/3/020>.
- [44] der Agobian R, Otto JL, Cagnard R, Echard R. Émission stimulée de nouvelles transitions infrarouges Dans Les Gaz Rares. *J Physique* 1964;25(10):887–97. <http://dx.doi.org/10.1051/jphys:019640025010088700>.
- [45] Gremmer W. Series in the xenon arc spectrum. *Z Phys* 1930;59(3–4):154–67. <http://dx.doi.org/10.1007/BF01341422>.
- [46] Chambers JM, Cleveland WS, Kleiner B, Tukey PA. Graphical methods for data analysis (vol 17, pg 180, 1983). *J Sleep Res* 2012;21(4):484. <http://dx.doi.org/10.1111/j.1365-2869.2011.00992.x>.
- [47] Faust WL, McFarlane RA, Patel CKN, Garrett CGB. Noble gas optical maser lines at wavelengths between 2 and 35 μ . *Phys Rev* 1964;133:A1476–86. <http://dx.doi.org/10.1103/PhysRev.133.A1476>.
- [48] Dasgupta A, Apruzese JP, Zatsarinny O, Bartschat K, Froese Fischer C. Laser transition probabilities in Xe I. *Phys Rev A* 2006;74:012509. <http://dx.doi.org/10.1103/PhysRevA.74.012509>.